Connector model for describing many-body interactions at surfaces

Yogesh Tiwary[1] and Kristen A. Fichthorn[1,2,*]
[1]*Department of Chemical Engineering, The Pennsylvania State University, University Park, Pennsylvania 16802, USA*
[2]*Department of Physics, The Pennsylvania State University, University Park, Pennsylvania 16802, USA*
(Received 16 August 2008; published 12 November 2008)

First-principles calculations based on density-functional theory indicate that high-order many-body interactions are significant in Al clusters on Al(110) and Al(100). The large number of many-body interactions renders a full-lattice-gas approach ineffective for such systems. To simplify the description of adsorbate interactions, we utilize two different schemes. First, we find effective parameters for Al adatom interactions using the leave-one-out cross-validation method. Second, we propose the connector model, which is based on additive single-atom connector units. The central idea of the connector model is to combine groups of many-body interactions into important structural units (e.g., step edges) that have a single interaction energy. We find that the connector model is more accurate and efficient in representing high-order many-body interactions than the traditional lattice-gas approach and it may be suitable for describing a variety of surface phenomena such as thin-film and crystal growth, adsorption, phase transitions, and catalysis at surfaces.

DOI: 10.1103/PhysRevB.78.205418 PACS number(s): 68.35.Md, 05.70.Np, 71.15.Nc, 81.10.Aj

I. INTRODUCTION

Achieving a predictive theoretical description of nanostructures that assemble at solid surfaces is important in a variety of applications, including electronic, magnetic, optical, and catalytic materials. A key element in this description is an accurate rendition of the interactions that govern assembly, which is a complex many-body problem. At the atomic scale, first-principles calculations based on density-functional theory (DFT) account for many-body effects and have been successful at elucidating the energetics that dictates structural evolution at surfaces. It is a current challenge to incorporate this information into computationally efficient models that can predict assembly on the mesoscopic and macroscopic scales. To this end, lattice-based models offer an attractive approach for many problems, as these retain the atomistic nature of the interface while allowing for an accurate albeit coarse-grained description of kinetics and interactions.

One of the most popular methods to coarse-grain atomic interactions is the lattice-gas model. In this model, the total interaction energy ΔE is given by a sum of pair, trio, and higher-order interactions among neighboring atoms; i.e.,

$$\Delta E = \sum_i \sigma_i E_{0,i} + \sum_i \sum_{j>i} \sigma_i \sigma_j E_2(i,j) + \sum_i \sum_{j>i} \sum_{k>j} \sigma_i \sigma_j \sigma_k E_3(i,j,k) + \cdots, \quad (1)$$

where $\sigma_{i(j,k)}=1$ if site i, j, or k is occupied and is 0 otherwise, $E_{0,i}$ is the adsorption energy of an atom on site i, $E_2(i,j)$ is the pair interaction between atoms on sites i and j, and $E_3(i,j,k)$ is the three-body interaction between three atoms on sites i, j, and k. The summation in Eq. (1) can be extended to four-body, five-body, and higher-order interactions. Rarely, however, are these interactions included and lattice-gas studies are typically based on effective pair interactions that are selected to match certain experimental attributes. While pair interactions may suffice for some studies, there has been a number of theoretical[1–8] and experimental[6,7,9] studies that have quantified adsorbate interactions and demonstrated that three-body and higher-order interactions can be significant. In this paper, we take up the issue of accurately and efficiently including these high-order many-body interactions into calculations of surface thermodynamics.

We consider the interactions between Al adatoms on the (110) and (100) surfaces of Al, which both occur in multilayer Al(110) homoepitaxy.[10] Al(110) homoepitaxy is a good example of the pervasive and essential role that many-body interactions can play in dictating surface thermodynamics. In a previous study, we used first-principles total-energy calculations to quantify 23 two- and three-body interactions that occur in dilute Al adlayers on Al(110).[4] Beyond the attractive nearest neighbor, the Al atom-pair interaction is repulsive[4] and it cannot explain experimentally observed nanostructures in Al/Al(110) homoepitaxy.[10] Some of the three-body interactions are attractive[4] and would promote the formation of experimentally observed nanostructures.[10] However, we will show in this work that in adsorbate clusters, four- and five-body interactions can be important on Al(110), as the magnitudes of these interactions are comparable to those of the most significant pairs and trios. We also obtain pair- and many-body interactions on Al(100) and find that the magnitudes of four- and five-body interactions are significant. Thus, our calculations indicate that the complete set of adsorbate interactions is large and untenable for lattice-gas calculations. It is possible to obtain an effective set of interactions using cross-validation (CV) methods[3,11–16] or the more recently introduced Bayesian statistics.[8] However, for the optimal sets of interactions on Al(110) and Al(100), the number of high-order many-body interactions is still significant. As an alternative to the lattice-gas model, we propose a "connector model," which has better accuracy than the best lattice-gas model we found using cross-validation methods, has fewer parameters than the full-lattice-gas (FLG) expansion, and can be efficiently incorporated in Monte Carlo (MC) simulations. We apply this model to study the energetics of adatom clusters on Al(110).

II. METHODS

We employed first-principles total-energy calculations based on DFT using the Vienna *ab initio* simulation package (VASP).[17–19] We utilized ultrasoft Vanderbilt-type pseudopotentials,[20] as supplied by Kresse and Hafner,[21] the generalized gradient approximation (GGA) by Perdew and Wang,[22] Fermi-Dirac smearing[23] with a width of 0.2 eV, and an energy cutoff of 9.50 Ry (129.2 eV) for the plane-wave basis set, which is sufficient for the desired accuracy. To sample the Brillouin zone, we used the Monkhorst-Pack scheme.[24] With a converged $(13\times13\times13)$ **k**-point mesh, we obtained a value for the bulk lattice constant of 4.05 Å, which is the same as the experimental value.[25]

To represent the Al(110) and Al(100) surfaces, we constructed supercells consisting of multilayered slabs with vacuum spacing above the surface, which are replicated periodically in the three orthonormal symmetry directions. For all the total-energy calculations, the vacuum spacing was greater than 15 Å, which is sufficient to avoid any interaction between the periodic slabs normal to the surface. We obtained optimized geometries by relaxing the unconstrained atoms in the slabs until the forces on all atoms became smaller than 0.01 eV/Å. The emergence of an artificial electric field perpendicular to the slab due to asymmetry is expected to be small for aluminum adatoms on aluminum surfaces.[4,26] Thus, we adsorbed atoms only on one side of the slab, which reduces the computational demands without compromising on the desired accuracy.

For Al(110), we used a converged slab thickness of 10 atomic layers, which was obtained in our previous work[4] by examining interlayer relaxations. To determine the necessary thickness of the Al(100) slab, we calculated interlayer relaxations using a 12-layer (1×1) slab. We allowed the top six layers to relax using a converged $(26\times26\times1)$ **k**-point mesh, while keeping atoms in the bottom six layers fixed at the bulk locations. We computed the interlayer relaxations $\Delta_{i,i+1}$, which are the percentage change from the bulk interlayer spacing between the i and $i+1$ layers, with $i=1$ for the top layer. We obtained $\Delta_{1,2}=1.76\%$ and $\Delta_{2,3}=0.67\%$, which are within the uncertainty of values found in recent low-energy electron diffraction (LEED) studies by Petersen *et al.*[27] ($\Delta_{1,2}=2.0\pm0.8\%$ and $\Delta_{2,3}=1.2\pm0.7\%$) and other theoretical studies.[28–31] Our value of $\Delta_{1,2}$ is also close to the LEED results by Berndt *et al.*[32] (1.84%), but we find that $\Delta_{2,3}$ is smaller than their value (2.04%). On Al(100), only the top two layers relax significantly and there are negligible relaxations associated with the third layer and beyond (e.g., $\Delta_{3,4}=0.27\%$). Hence, we used an eight-layer slab for Al(100), with the top four layers and adatoms unconstrained. For the eight-layer slab, we obtained $\Delta_{1,2}=1.50\%$ and $\Delta_{2,3}=0.36\%$, which are still in reasonable agreement with LEED results.[27]

In our previous study of Al adatom interactions on Al(110), we used slabs with (5×3) and (3×5) surface atoms along the $([1\bar{1}0]\times[001])$ (in-channel×cross-channel) directions, with converged $(5\times6\times1)$ and $(8\times3\times1)$ **k**-point meshes, respectively.[4] To accommodate larger adsorbate geometries in this work, we adopted a somewhat larger slab for Al(110), which has (8×5) surface atoms. For this slab, we used a $(4\times4\times1)$ **k**-point mesh, which has a higher **k**-point density than that in our previous study.[4] We maintained this approximate **k**-point density for the other slabs in this work. Similarly, for Al(100) the largest slab has (7×7) surface atoms, for which we use a $(4\times4\times1)$ **k**-point mesh. We determined the suitability of this **k**-point mesh by calculating the values of the adsorption energy E_{ads} for an Al adatom on a $(7\times7\times8)$ slab. The adsorption energy is defined as

$$E_{ads}=E_{s+1}-E_s, \tag{2}$$

where E_{s+1} is the energy of a relaxed slab containing one adatom and E_s is the energy of the bare relaxed slab. To calculate the adsorption energy, we employed $(2\times2\times1)$, $(3\times3\times1)$, $(4\times4\times1)$, and $(5\times5\times1)$ **k**-point meshes. The adsorption energy converged (within 1 meV) to a value of $E_{ads}=-3.332$ eV for the $(4\times4\times1)$ **k**-point mesh. We used approximately the same **k**-point density for other Al(100) slabs in this work.

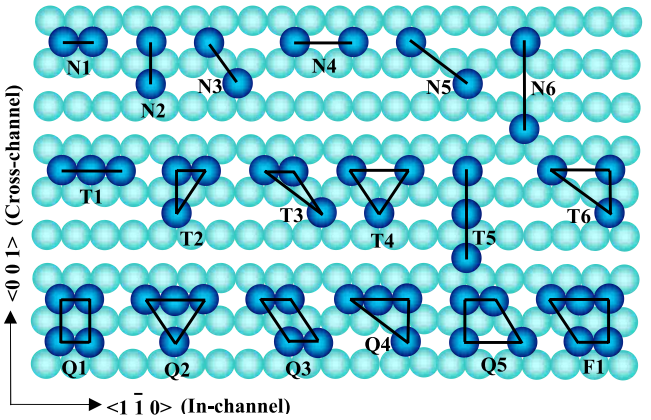

FIG. 1. (Color online) Four-body (*Qi*) and five-body (*Fi*) interactions on Al(110) along with associated pairs (*Ni*) and trios (*Ti*).

III. LATTICE-GAS MODEL

We first characterized interactions between adsorbed atoms and their origins within the framework of the lattice-gas model. In the lattice-gas approach, the total interaction energy or lattice-gas Hamiltonian (LGH) is expressed as the sum of the involved two-, three-, and higher-body interaction terms [cf. Eq. (1)]. The total interaction energy ΔE can be obtained from DFT calculations as

$$\Delta E=E_{s+N}-E_s-NE_{ads}, \tag{3}$$

where E_{s+N}, E_s, and E_{ads} are the energies of the slab with N adatoms, the bare slab, and the adsorption energy of a single adatom on the slab [defined in Eq. (2)], respectively. We used an $(8\times5\times10)$ slab for Al(110) and a $(7\times7\times8)$ slab for Al(100) in these calculations. In this work, we quantified five four-body and one five-body interactions along with the related pair and trio interactions. These are shown in Figs. 1 and 2 for Al(110) and Al(100), respectively. In these figures, the pairs that are *i*th nearest neighbors are denoted as *Ni*, while trios, four-body, and five-body interactions are denoted

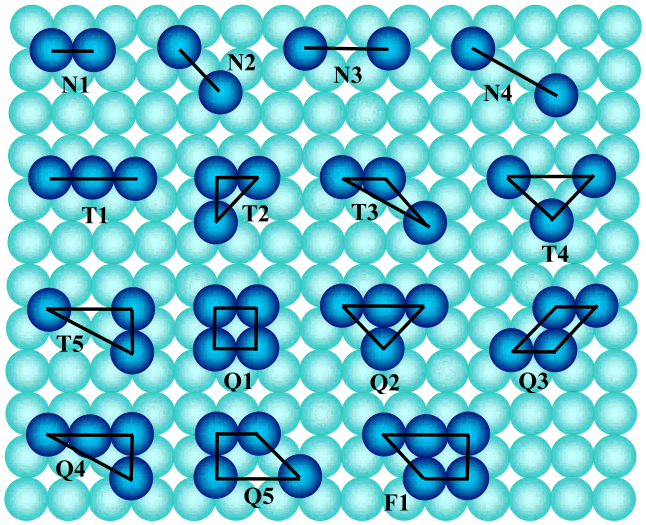

FIG. 2. (Color online) Four-body (Qi) and five-body (Fi) interactions on Al(100) along with associated pairs (Ni) and trios (Ti).

as Ti, Qi, and Fi, respectively. The corresponding interaction energies are denoted as E_{Ni}, E_{Ti}, E_{Qi}, and E_{Fi}. The total interaction energy for each of the configurations in Figs. 1 and 2 can be expressed as a sum involving some of the interactions. For example, the total interaction energy for the four-atom cluster $Q2$ on Al(110) (Fig. 1) is given by

$$\Delta E = 2E_{N1} + E_{N2} + 2E_{N3} + E_{N4} + E_{T1} + 2E_{T2} + E_{T4} + E_{Q2}. \quad (4)$$

Although interactions between adatoms and their periodic images can be important if the slab dimensions are small compared to the interaction range,[4,33–35] we verified that this is not the case here. We obtain a similar equation for each of the clusters shown in Figs. 1 and 2 and we solve the resulting set of linear equations to obtain the interaction energies. The results are shown in Table I.

Adsorbate interactions can be direct or indirect and mediated by the substrate.[4,36–50] Indirect substrate-mediated interactions can have electronic and/or elastic origins. To resolve the origins of the interactions, we used an approach adopted in previous studies[4,33,34,51] in which we employed two different relaxation schemes. In the first set of calculations, the adatoms and substrate atoms [five layers for Al(110) and four layers for Al(100)] were allowed to relax, while in the second scheme we allowed the adatoms to relax on a fixed substrate in which the atoms assume their relaxed positions for a bare surface. In the second scheme, we suppress relaxation of the surface with respect to the adatoms and we obtain the electronic component of the interactions. This component was subtracted from the total interaction energies obtained in the first scheme to estimate the elastic component. We note that this scheme does not perfectly delineate electronic and elastic interactions because the two may be coupled—especially when direct chemical bonds are formed. Nevertheless, it provides some resolution of the two different modes.

We quantified all the relevant pair and trio interactions on Al(110) in a previous study[4]—the values reported in Table I are slightly different than those (rms error of 0.012 eV) due to differences in the slab size and **k**-point sampling. On Al(110), the nearest-neighbor pair interaction ($N1$) is the strongest and is electronic in nature. This interaction reflects the formation of a direct chemical bond between in-channel

TABLE I. Values of the total, electronic, and elastic components of interaction energies for the configurations shown in Figs. 1 and 2. A negative value of the interaction energy denotes attraction.

	Interaction energy (eV)					
	Al(110)			Al(100)		
	Total	Electronic	Elastic	Total	Electronic	Elastic
$N1$	−0.091	−0.241	0.150	−0.255	−0.238	−0.017
$N2$	0.050	−0.004	0.053	0.037	−0.004	0.041
$N3$	0.043	0.007	0.036	0.017	0.007	0.011
$N4$	0.045	0.002	0.043	0.010	0.001	0.009
$N5$	0.036	0.001	0.035			
$N6$	0.010	−0.004	0.014			
$T1$	−0.006	0.057	−0.063	0.066	0.013	0.053
$T2$	−0.057	−0.006	−0.051	0.083	0.070	0.012
$T3$	−0.049	−0.004	−0.045	−0.018	−0.012	−0.006
$T4$	−0.026	−0.002	−0.025	−0.013	0.000	−0.012
$T5$	0.005	0.008	−0.003	−0.006	−0.006	0.001
$T6$	−0.025	−0.001	−0.024			
$Q1$	0.071	0.010	0.060	−0.074	−0.086	0.012
$Q2$	0.042	−0.003	0.045	−0.054	−0.042	−0.013
$Q3$	0.051	−0.004	0.054	−0.028	−0.037	0.009
$Q4$	0.034	0.001	0.034	−0.035	−0.008	−0.026
$Q5$	0.027	0.001	0.027	0.004	−0.004	0.008
$F1$	−0.045	0.000	−0.045	0.013	0.041	−0.028

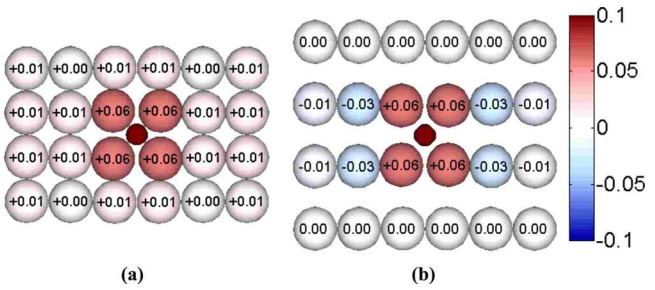

FIG. 3. (Color online) Relaxations of the relevant surface atoms (normal to the surface plane) induced by the presence of an adatom on (a) Al(100) and (b) Al(110). The small circles in the center show the position of the adatom and the heights (in angstrom) of the surrounding surface atoms relative to those of the bare surface are indicated on the color scale.

nearest-neighbor Al atoms. The pair interactions beyond the nearest neighbor are repulsive and have elastic origins. Interestingly, we find a similar trend for pair interactions on Al(100). However, the interaction range is shorter on Al(100) than on Al(110).

In our previous study of Al(110),[4] we could understand the range of the pair interaction in terms of an elastic perturbation zone surrounding an isolated adatom. An adsorbed atom perturbs the positions of surface atoms surrounding it. The range over which this perturbation is significant determines the range of the elastic interaction with other adatoms. Figure 3(a) shows the most significant perturbations of the substrate atoms in the first layer of a $(7\times7\times8)$ Al(100) slab, along with the results for an adatom on an $(8\times5\times10)$ Al(110) slab [Fig. 3(b)]. We see that for Al(100), the four base atoms in contact with the adatom relax upward toward the adatom relative to those on a bare surface. Beyond this base, the perturbation of the substrate is insignificant. Although the normal perturbations of the four base atoms below the adatom are similar on Al(100) and Al(110), the Al(110) surface exhibits an anisotropic and oscillatory response to the adatom, with nearest-neighbor surface atoms to the four base atoms along the cross-channel direction exhibiting virtually no relaxation and neighbors along the in-channel direction exhibiting an oscillatory relaxation that extends to the second-neighbor surface atoms. The maximum range of the elastic interaction can be estimated as two times the size of the perturbation zone for an adatom; i.e., if the perturbation zones of two adatoms do not touch or overlap then they are essentially isolated adatoms. Thus, for Al(110), the range of the pair interaction is ~8 Å or *N*6 on Al(110). On Al(100), the pair interactions have a smaller range of ~6.4 Å or the fourth-nearest neighbor.

Trio interactions are significant on both surfaces—although they have different origins on Al(110) and Al(100). On Al(110), all trio interactions except for the collinear trio (*T*1) are elastic in origin.[4] Here, we report on trio energies up to *T*6; however, the trio interaction on Al(110) extends to a longer range than this.[4] The trios on Al(100) are more complex than those on Al(110) and most have both electronic and elastic components. It is evident that four- and five-body interactions are also significant on both surfaces. These high-order interactions are primarily elastic in origin on Al(110). As the trios, the four- and five-body interactions on Al(100) contain both elastic and electronic components. The most compact quarto *Q*1 is the strongest on both the surfaces, and the magnitude decreases for more open clusters *Q*4 and *Q*5. There is no indication of the convergence of interaction energies as we move to higher-order interactions. In fact, some of four- and five-body interactions have higher magnitudes than the three-body interactions.

For the lattice-gas model to be efficient, the number of high-order many-body terms should be limited. Here, we quantified 18 significant interaction terms for Al(110) and 15 terms for Al(100). Although we can consider this to be a complete set of interactions for the clusters shown in Figs. 1 and 2, there is no guarantee that this set of interactions will suffice to describe the energetics of other adsorbate structures. In particular, we know that for Al(110) there are 23 significant pair and trio interactions[4] that could become important if we consider structures other than those shown in Fig. 1. Further, there is no reason to assume that other prospective five- and higher-body terms, not considered in this work, are not significant. Such a large number of significant terms makes the lattice-gas approach unwieldy. Below, we consider alternatives to the full-lattice-gas approach.

IV. LATTICE-GAS MODEL WITH EFFECTIVE PARAMETERS

In recent studies, various search algorithms have been employed to reduce the set of interaction terms in lattice-gas models or cluster expansions by obtaining an optimal set of effective parameters.[3,8,11–16] This involves least-squares fitting of trial LGH to predetermined DFT energies for a large number of atomic configurations and using the minimum number of interaction terms possible to achieve a desired accuracy. A subset of n interactions (pairs, trios, etc.) is chosen from a larger set of N possible interactions. To determine the optimal subset of n interactions, we employ the leave-one-out cross-validation method.[3,11–14] In this method, we select a set of n interactions and we do a least-squares fitting of a trial LGH to $M-1$ DFT configurations/energies (out of M total) to obtain the values of the interaction energy terms. The remaining DFT configuration i is used to assess the lattice-gas prediction $E^{\mathrm{LGH}}(i)$ relative to the corresponding DFT value $E^{\mathrm{DFT}}(i)$. A CV score is obtained for the interaction terms selected as

$$\mathrm{CV} = \sqrt{\frac{1}{M}\sum_{i=1}^{M}\{[E^{\mathrm{DFT}}(i) - E^{\mathrm{LGH}}(i)]^2\}}. \tag{5}$$

We repeat this procedure for different sets of n interactions—with N possible terms, we repeat it $\binom{N}{n}$ times—and the optimal set of n interactions emerges as the one with the minimum CV score. The interaction parameters in this optimal set are fit to all M DFT configurations to obtain the final set of interactions. We then repeat the procedure for different values of n. The goal is to minimize the value of n while keeping the CV score low.

We tested the leave-one-out cross-validation scheme for Al(110) and Al(100) beginning with the interactions shown

TABLE II. Al(110) interaction energies obtained by solving FLG equations (i.e., those shown in Fig. 1 and Table I) and least-squares fitting with n interaction terms. Terms that were eliminated are indicated by dots. Also shown are the CV scores and the maximum errors ϵ between the LGH predictions and the DFT values of total interaction energies for 32 configurations. For the FLG and connector models, the CV scores are given as the rms error between the model predictions and DFT values.

	Interaction energy (eV)						
	FLG	$n=18$	$n=14$	$n=10$	$n=6$	$n=4$	Connector
$N1$	−0.091	−0.086	−0.092	−0.095	−0.093	−0.094	·
$N2$	0.050	0.050	0.052	0.053	0.053	0.062	·
$N3$	0.043	0.047	0.046	0.044	0.025	·	·
$N4$	0.045	0.045	0.040	0.045	0.039	0.041	·
$N5$	0.036	0.009	·	·	·	·	·
$N6$	0.010	0.010	0.010	0.009	0.011	·	·
$T1$	−0.006	−0.015	·	·	·	·	·
$T2$	−0.057	−0.067	−0.062	−0.052	−0.033	−0.021	·
$T3$	−0.049	−0.030	−0.015	−0.008	·	·	·
$T4$	−0.026	−0.038	−0.030	−0.032	·	·	·
$T5$	0.005	0.003	0.000	·	·	·	·
$T6$	−0.025	0.002	0.014	·	·	·	·
$Q1$	0.071	0.093	0.081	0.052	·	·	·
$Q2$	0.042	0.067	0.050	0.039	·	·	·
$Q3$	0.051	0.044	0.023	·	·	·	·
$Q4$	0.034	0.023	·	·	·	·	·
$Q5$	0.027	0.022	·	·	·	·	·
$F1$	−0.045	−0.058	−0.023	·	·	·	·
CV	0.014	0.021	0.009	0.009	0.013	0.020	0.007
ϵ(eV/atom)	0.030	0.014	0.018	0.018	0.018	0.022	0.006

in Figs. 1 and 2, respectively, as these seem likely to be the most significant ones. To fit and test possible LGH, we obtained the total interaction energies for M configurations [$M=32$ for Al(110) and $M=28$ for Al(100)] using DFT calculations. We tried all possible combinations for n interaction terms, out of $N=18$ for Al(110) and $N=15$ for Al(100), to construct LGH and obtained the interaction energies of these terms using the combination which gives the minimum CV score. We varied n from 18 to 1 for Al(110) and 15 to 1 for Al(100). Tables II and III show the resulting values of the interaction energies for a few values of n, corresponding CV scores, and the maximum difference (per atom) ϵ in the total interaction energy with respect to DFT values, which is given by

$$\epsilon = \max_{i=1}^{M} \left[\frac{E^{\mathrm{DFT}}(i) - E^{\mathrm{LGH}}(i)}{N(i)} \right], \tag{6}$$

where $N(i)$ is the number of adatoms in the ith configuration. Similar to previous studies,[3,14] we find that CV scores are high for large values of n, decrease for moderate values, and again increase for small n.

Based on CV scores and maximum errors, we see that the optimal interaction sets for Al(110) have ~6–14 interaction parameters while those for Al(100) have ~5–12. Three-body and higher interactions figure prominently in both sets of interactions. The actual interaction energies obtained from the FLG formulation are also given in Tables II and III. Here we see that even though the FLG model exactly describes the energies of the structures in Figs. 1 and 2, it does a poor job at describing the test structures, which contain other interactions. On the other hand, it is clear that the interaction energies obtained by fitting are mostly different from the FLG values that describe the clusters in Figs. 1 and 2. This is because the effective values compensate for interaction terms missing in the effective sets as well as those missing from the FLG in the additional DFT configurations. While this loss of accuracy may be acceptable for certain applications, we strive for a physically motivated model with greater accuracy and good efficiency for Monte Carlo studies. Below, we describe a model (the connector model) that achieves this goal.

V. CONNECTOR MODEL

To efficiently capture many-body interactions at surfaces, we present a connector model. In the connector model, structures are formed from sets of building blocks called connectors. Here, connectors are single-atom units with bonds that link them to neighboring atoms. The total energies of structures at surfaces are obtained by summing the connector binding energies. For example, the set of the connectors

TABLE III. Al(100) interaction energies obtained by solving FLG equations (i.e., those shown in Fig. 2 and Table I) and least-squares fitting with n interaction terms. Terms that were eliminated are indicated by dots. Also shown are the CV scores and the maximum errors ϵ between the LGH predictions and the DFT values of total interaction energies for 28 configurations. For the FLG and connector models, the CV scores are given as the rms error between the model predictions and DFT values.

	Interaction energy (eV)						
	FLG	$n=15$	$n=12$	$n=8$	$n=5$	$n=4$	Connector
$N1$	−0.255	−0.221	−0.221	−0.216	−0.217	−0.220	·
$N2$	0.037	0.033	0.035	0.037	0.039	0.035	·
$N3$	0.017	0.007	·	·	·	·	·
$N4$	0.010	0.001	−0.003	−0.007	·	−0.016	·
$T1$	0.066	0.009	0.015	·	·	·	·
$T2$	0.083	0.033	0.029	0.022	0.022	0.026	·
$T3$	−0.018	−0.028	−0.031	−0.026	−0.029	·	·
$T4$	−0.013	0.006	0.009	·	·	·	·
$T5$	−0.006	−0.010	·	·	·	·	·
$Q1$	−0.074	−0.025	−0.016	·	·	·	·
$Q2$	−0.054	−0.016	−0.016	0.009	·	·	·
$Q3$	−0.028	0.000	0.010	·	·	·	·
$Q4$	−0.035	−0.001	·	·	·	·	·
$Q5$	0.004	0.010	0.010	0.010	·	·	·
$F1$	0.013	0.021	0.009	0.007	0.021	·	·
CV	0.412	0.079	0.018	0.015	0.015	0.020	0.011
ϵ(eV/atom)	0.191	0.017	0.017	0.023	0.024	0.031	0.007

needed to describe rectangular clusters and atom chains on Al(110) is shown in Fig. 4. In Fig. 4, C1 represents an isolated atom, while C2 and C3 are needed to describe dimers or the ends of atom chains along the in-channel $[1\bar{1}0]$ and cross-channel [001] directions, respectively. C4 and C5 model atoms inside atom chains along the in- and cross-channel directions, C6 represents corners of compact Al islands, C7 and C8 model the close-packed step edges, and C9 models atoms that have a full complement of first, second, and third neighbors in the surface plane such as those in the interior of an adsorbate island or within the first layer of surface atoms. Also shown in Fig. 4 are the binding and interaction energies of C1–C9, which are obtained in DFT calculations.

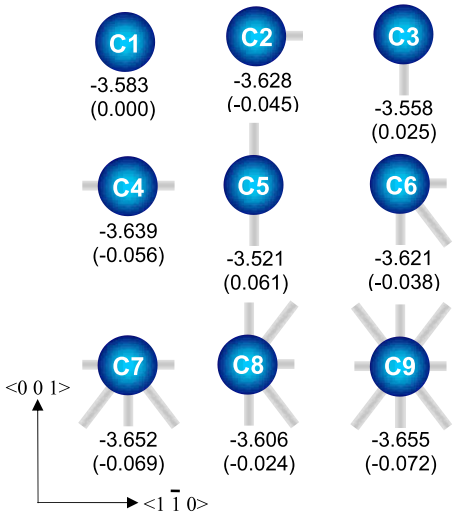

FIG. 4. (Color online) The connectors in compact rectangular islands and adatom chains on Al(110), along with their binding and interaction energies (the binding energy minus the binding energy of C1) in units of eV.

Figure 5 shows a few examples of how connector binding energies are obtained. We obtain the binding energy B_{C9} for C9 as the difference between the energy E of a $(1\times1\times11)$ slab and that of a $(1\times1\times10)$ slab $E_s^{1\times1}$. The binding energy of C5 B_{C5} comes from a semi-infinite atom chain along the [001] direction and is given by the difference between the

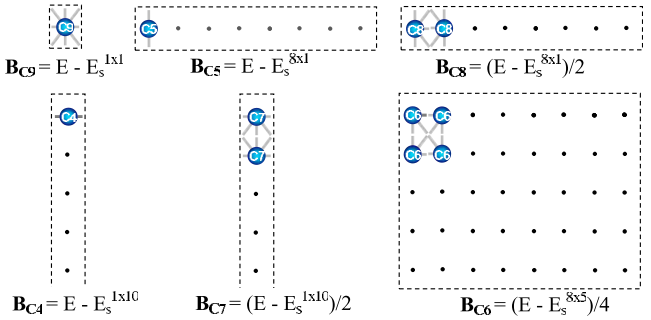

FIG. 5. (Color online) A few slabs and adatom configurations used to obtain the binding energies B_{Ci} of Al(110) connectors. Here, E is the total energy of the slab plus adatoms and E_s is the energy of a bare slab with superscripts indicating the size of slabs. The full slab is not shown for B_{C4} and B_{C7}.

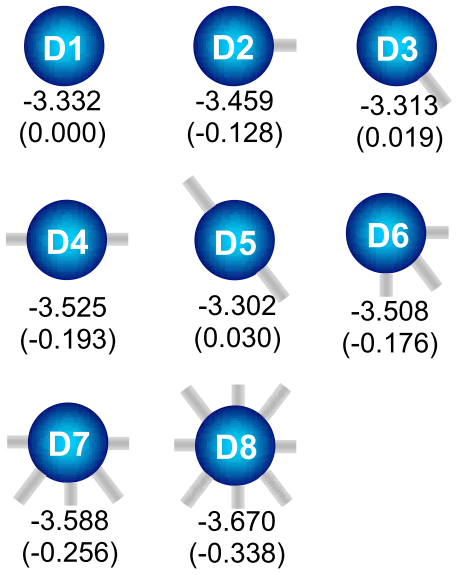

FIG. 6. (Color online) The connectors in compact square and rectangular islands and adatom chains on Al(100), along with their binding and interaction energies (the binding energy minus the binding energy of D1) in units of eV.

energy E of an (8×1) slab with a single atom and a bare (8×1) slab $E^{8\times1}$. Similarly, we obtain B_{C8} from a semi-infinite chain along the [001] direction that is two atoms wide. Since, as shown in Fig. 5, such a configuration contains two C8 units, we have $B_{C8}=(E-E^{8\times1})/2$. The binding energies of C4 and C7 can be obtained in an analogous way to those of C5 and C8. Finally, we obtain B_{C6} from one fourth of the difference between the energy of an (8×5) slab with a four-atom rectangle and the energy of a bare (8×5) slab, as shown in Fig. 5. Using a similar methodology, we obtain the binding energies of Al(100) connectors D1–D8 which are reported in Fig. 6.

Although the connectors in Figs. 4 and 6 do not constitute a complete set that could describe the configuration of any adlayer, they do represent important building blocks for nanostructures at surfaces and their energies can be related to important physical quantities. For example, the energies of C9 and D8 both represent the bulk cohesive energy. These values should be the same and the small difference between the two can be attributed to the differences in **k** points and slab thickness in the calculations for Al(110) and Al(100). These values are in reasonable agreement with previously calculated values from DFT.[26,30] The C7 and C8 connectors represent the (111)- and the (100)-faceted steps on Al(110), respectively, and D7 represents the (111)-faceted step on Al(100). These connectors can yield the step energies λ if we subtract the bulk cohesive energies from their binding energies. On Al(110), we obtain the step energies as $\lambda_{(111)}=0.003$ eV/atom and $\lambda_{(100)}=0.048$ eV/atom, and on Al(100) we obtain $\lambda_{(111)}=0.082$ eV/atom. These are in general agreement with theoretical[52–57] and experimental[58] values for other unreconstructed fcc surfaces. The corner energies C6 and D6 play a role in determining the shapes of small islands. By comparing the energies of C1 and D1, we find that an isolated adatom has a stronger surface binding on

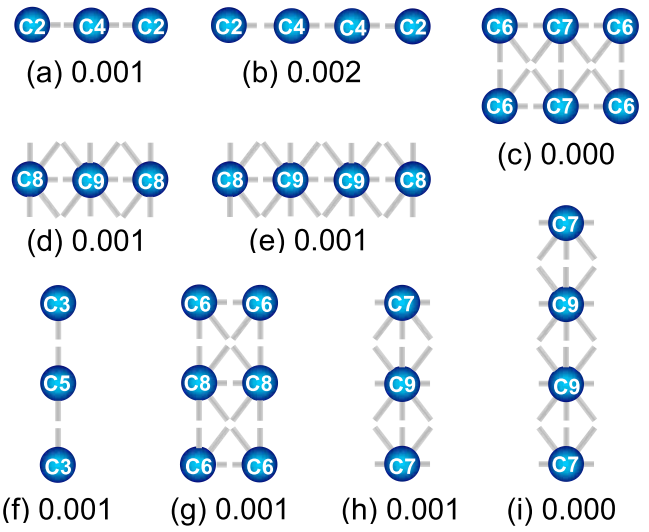

FIG. 7. (Color online) Test clusters for Al(110) along with the difference (in eV/atom) between *ab initio* and connector-model energies. The structures in (d), (e), (h), and (i) are semi-infinite.

Al(110) compared to Al(100). These binding energies reflect the surface energies of Al(110) and Al(100), which (for the slabs studied here) we find to be $\gamma_s=0.57$ and 0.429 eV/atom, respectively. These values are close to those found in experimental[59] studies and reasonably close to values found in other theoretical[26,30,60] studies—differences can be attributed to differences in slab thickness [for a 50-layer slab, we find $\gamma_s=0.665$ eV/atom for Al(110) and for a 20-layer slab, we find $\gamma_s=0.454$ eV/atom for Al(100)] as well as the exchange-correlation functional and choice of pseudopotential.

Comparing connectors to interactions within the lattice-gas approach, we note that the interaction energies associated with the "one-armed" connectors C2, C3, D2, and D3 are half the interaction energies of their corresponding pair in the FLG model (cf. Figs. 1 and 2 and Tables II and III). Connectors with more than two arms incorporate multiple interactions. For example, C6 reflects at least three different pair interactions and at least one type of trio and four-body interaction, while C9 contains, among others, a nine-body interaction. By combining units that incorporate groups of interactions, we can include important high-order many-body interactions, describe the energies of important structural units, and, as we will discuss below, achieve greater computational efficiency.

To test the connector model, we compare the total energies for nine compact Al(110) and Al(100) clusters obtained by *ab initio* DFT calculations with the connector-model predictions. The clusters used to test the Al(110) connectors are shown in Fig. 7, along with the corresponding differences from the DFT calculations in eV/atom. To obtain the connector-model binding energies for the clusters, we simply identify the connectors associated with each of the atoms in the cluster and we sum their energies. For example, the binding energy per atom of the atom chain in Fig. 7(a) is given by $(2B_{C2}+B_{C4})/3$ and that of the semi-infinite strip in Fig. 7(d) is $(2B_{C8}+B_{C9})/3$.

From Fig. 7, we see that although connectors integrate high-order many-body interactions, their range appears to be

limited to the third neighbor in adsorbate clusters. For example, although C4 was obtained from a calculation involving an infinite adatom chain (cf. Fig. 5), it effectively reproduces the energies of finite structures [cf. Figs. 7(a) and 7(b)]. Similarly, C5, C7, and C8 were obtained from semi-infinite structures (cf. Fig. 5) but they accurately reproduce the energies of finite structures, while C9, the "bulk" connector, works well in various semi-infinite environments. Although C6 was obtained from a four-atom cluster (cf. Fig. 5), it is effective in describing the energies of the six-atom clusters in Figs. 7(c) and 7(g). From Fig. 7, we see that the maximum error is only 0.002 eV/atom. Further considerations indicate that the test clusters in Fig. 7 along with the fitting clusters, some of which are shown in Fig. 5, form a complete set that ranges from (semi-) infinite structures to the most finite structures possible. Thus, we would not expect the quality of the agreement with DFT to diminish with the introduction of further test clusters and we can conclude that for chains and rectangular structures, the connector model is as good as DFT. We used similar clusters to test the connector model on Al(100), where we find a maximum error of 0.003 eV/atom and we reach the same conclusion about the accuracy on that surface.

With the connectors given in Fig. 4, we can consider the role of many-body interactions in promoting island shapes on Al(110). Considering just pair interactions, the only stable structures are linear atom chains along the $[1\bar{1}0]$ direction, as the only attractive pair interaction is the nearest neighbor along this direction[4] (cf. Table I). Nevertheless, we find, due to many-body effects, that two-dimensional (2D) islands become energetically preferred for sufficiently large islands. To probe the stability of 2D islands, we fix the [100] width m of an adatom cluster and increase the $[1\bar{1}0]$ length n to find the minimum value $n_{\min}$ for which an $n_{\min}\times m$ cluster becomes more stable than a cluster with a width of $(m-1)$ and the same number of atoms. For example, the value of $n_{\min}=4$ for $m=2$ because 1×2, 2×2, and 3×2 clusters are less stable than the 2×1, 4×1, and 6×1 atom chains, respectively, but a 4×2 cluster is more stable than an 8×1 chain. Figure 8 shows the value of $n_{\min}$ along with the corresponding island aspect ratio for various values of m. For large islands, the aspect ratio converges to ~16, as predicted using the Wulff construction,[61] i.e., $\lambda_{(100)}/\lambda_{(111)}=16.0$ (number basis) or 11.88 (length basis). Similar aspect ratios can be inferred from theoretical calculations[52–56,62] and have been observed experimentally[63–66] for other fcc(110) surfaces. Interestingly, the aspect ratio for small islands is smaller than the Wulff value. This is due to the effect of corner atoms, which are not considered in the Wulff construction, and the discreteness of the clusters, as many atoms are necessary to achieve the Wulff aspect ratio.

The connector model is not limited to square and rectangular geometries and it can be extended. To efficiently determine the relevant connectors, we can make some justified assumptions based on our observations. From a few trial calculations for Al(110), we observed that the second- (cross-channel) and third-neighbor (diagonal) interactions are essentially identical and distinct from the first-neighbor (in-channel) interaction. Thus, we can categorize the Al(110)

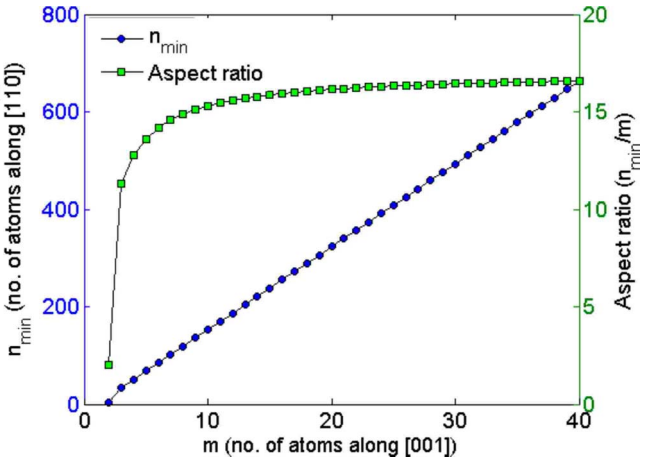

FIG. 8. (Color online) Number of atoms along the $[1\bar{1}0]$ direction $n_{\min}$ and aspect ratio $(n_{\min}/m)$ vs m (atoms along the [001] direction) for clusters on Al(110).

connector arms as in-channel A arms and cross-channel or diagonal B arms. Also, we find that the connector binding energies are approximately independent of the arrangement of the type B bonds on this surface—with good accuracy, they depend only on the number of B bonds. Thus, we can denote all the Al(110) connectors by a connector matrix $\mathbf{C}(N_B,N_A)$, where N_A and N_B are the number of bonds of type A and B, respectively. For example, C9=$\mathbf{C}(6,2)$ and C2 =$\mathbf{C}(0,1)$. In this framework, there are 21 connectors for $N_A=0-2$ and $N_B=0-6$. The connector matrix, with binding energies in eV, is given by

$$\mathbf{C}(N_B,N_A)=\begin{pmatrix} \underline{\mathbf{-3.583}} & \underline{\mathbf{-3.628}} & \underline{\mathbf{-3.639}} \\ \underline{\mathbf{-3.558}} & \underline{\mathbf{-3.641}} & -3.644 \\ \underline{\mathbf{-3.521}} & \underline{\mathbf{-3.621}} & -3.649 \\ \underline{\mathbf{-3.519}} & -3.619 & \underline{\mathbf{-3.652}} \\ \underline{\mathbf{-3.445}} & \underline{\mathbf{-3.606}} & -3.654 \\ -3.400 & -3.587 & -3.654 \\ -3.337 & -3.563 & \underline{\mathbf{-3.655}} \end{pmatrix}. \quad (7)$$

We calculated the binding energies of 12 connectors using DFT [bold and underlined in Eq. (7)] and obtained the rest by fitting a second-order polynomial to each of the columns in $\mathbf{C}(N_B,N_A)$. From the connector matrix in Eq. (7), we see that for a fixed number of cross-channel or diagonal B bonds, the connector binding energies always increase in magnitude with the number of in-channel A bonds. Interestingly many-body effects can be seen in the variation in the connector binding energies with the number of B bonds: with no A bonds, the connector binding energies decrease in magnitude as N_B increases; with one A bond, they go through a maximum; and with two A bonds, the connector binding energy increases in magnitude with N_B and levels at bulk cohesive energy as we reach a full complement of A and B bonds.

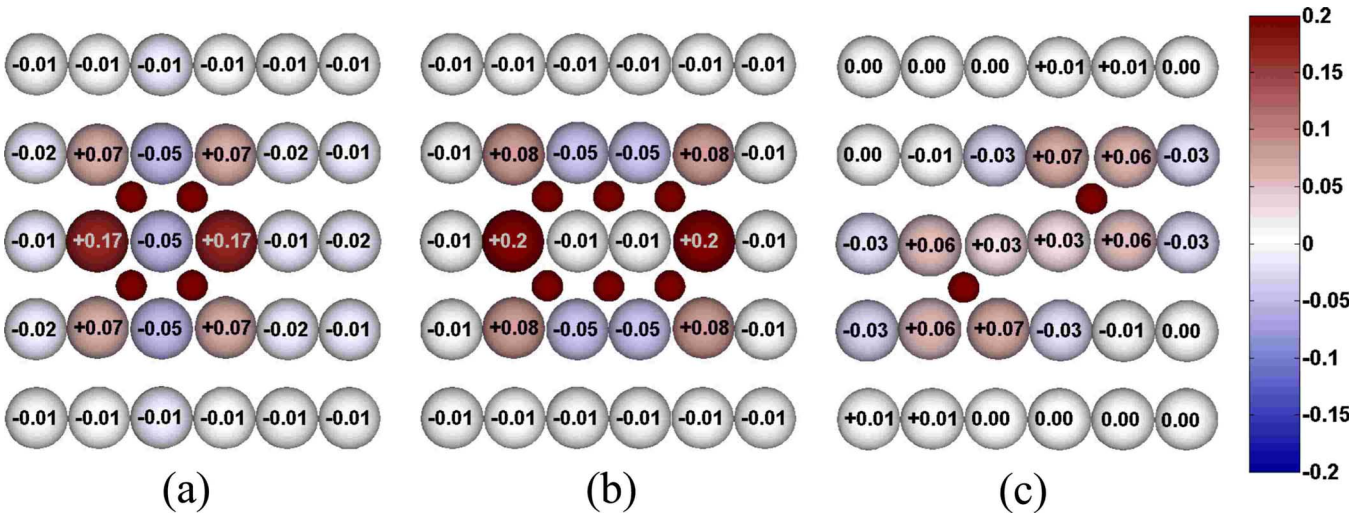

FIG. 9. (Color online) Change in the height (in angstrom) of top-layer surface atoms relative to those on a bare relaxed Al(110) surface for a surface containing (a) a four-atom cluster, (b) a six-atom cluster, and (c) an atom pair. The small circles represent adatoms.

On Al(100), we also found that the connector energies are essentially independent of the arrangement of the nearest- and next-nearest-bonds. Thus, similar to Al(110), the connectors can be denoted by $\mathbf{D}(N_B,N_A)$, where N_A and N_B are the numbers of nearest- and next-nearest-bonds, respectively. Thus, we have 25 connectors corresponding to $N_A=0-4$ and $N_B=0-4$. The connector matrix with binding energies in eV for Al(100) is given by

$$\mathbf{D}(N_B,N_A)=\begin{pmatrix} \underline{\mathbf{-3.332}} & \underline{\mathbf{-3.459}} & \underline{\mathbf{-3.525}} & \underline{\mathbf{-3.561}} & -3.608 \\ \underline{\mathbf{-3.313}} & \underline{\mathbf{-3.431}} & \underline{\mathbf{-3.508}} & -3.577 & -3.637 \\ \underline{\mathbf{-3.302}} & -3.415 & \underline{\mathbf{-3.517}} & \underline{\mathbf{-3.588}} & -3.658 \\ -3.299 & -3.404 & -3.504 & -3.589 & -3.668 \\ -3.298 & -3.395 & -3.491 & -3.583 & \underline{\mathbf{-3.670}} \end{pmatrix}. \tag{8}$$

We calculated 11 connector binding energies using DFT [bold and underlined in Eq. (8)] and obtained the rest using local piecewise triangle (linear) interpolation. Similar to the Al(110) connectors, the connectors in Eq. (8) show a complex many-body dependence on the number of nearest- and next-nearest-neighbor bonds.

It is a property of adsorbed structures on these surfaces that interactions among atoms in dilute clusters have a longer range than those in dense clusters. Long-range pair interactions in these systems are elastic in origin (cf. Table I) and there are significant differences between two atoms that are part of a cluster and two adatoms that do not share direct bonds. Figures 9 and 10 illustrate this trend. Comparing the relaxations associated with the corner atoms in the four- and six-atom clusters in Figs. 9(a) and 9(b) and Figs. 10(a) and 10(b), we see that these are similar and consistent with short-range bonding in dense clusters. However, comparing the corner relaxation for the six-atom clusters to those associated with the atom pairs [Figs. 9(b) and 9(c) and Figs. 10(b) and 10(c)], we see that the substrate relaxations leading to the elastic interactions between these two adsorbate pairs (cf. Table I) are substantially different when the atoms are part of a six-atom cluster. The significant alteration of the long-range elastic interaction, due to short-range surface relaxation and direct chemical bonding, is one of the origins of the many-body interactions on these surfaces.

To describe both dense and dilute adlayer structures, we need to account for long-ranged pair interactions in dilute clusters. For this purpose, we introduce two connectors shown in Figs. 11(a) and 11(b) ($N4$ and $N5$) for Al(110) and Figs. 11(c) and 11(d) ($N3$ and $N4$) for Al(100). These connectors describe pairs with the dilute local environments shown in Fig. 11. With the connectors in Fig. 11, as well as those in the connector matrices in Eqs. (7) and (8), we have a complete description of the first layer in homoepitaxy on Al(110) and Al(100).

To test the connector model, we applied it to 32 adatom configurations on Al(110) and 28 on Al(100). These are the same structures used to test the lattice-gas model in Sec. IV. We also obtained CV scores as the rms error between the

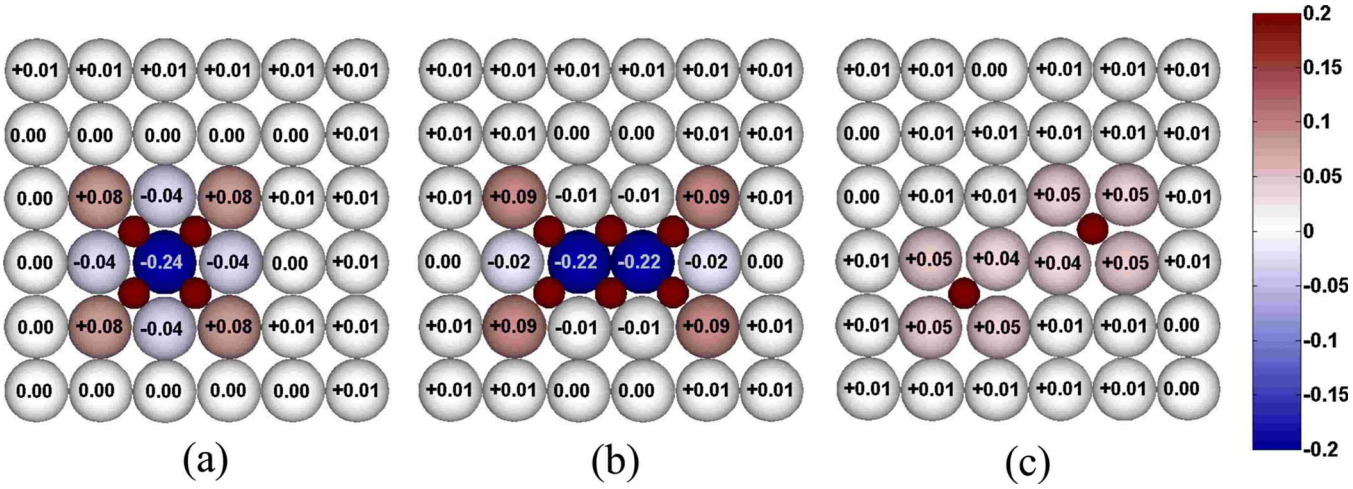

FIG. 10. (Color online) Change in the height (in angstrom) of top-layer surface atoms relative to those on a bare relaxed Al(100) surface for a surface containing (a) a four-atom cluster, (b) a six-atom cluster, and (c) an atom pair. The small circles represent adatoms.

connector-model predictions and the DFT energies. These are reported in Tables II and III along with the maximum errors for the connector model. Some additional test structures are shown in Fig. 12 along with the differences from DFT results. In Tables II and III, as well as in Fig. 12, we can see that for both Al(110) and Al(100) the CV scores and maximum errors associated with the connector model are lower than those for the best models with effective interactions. In particular, the maximum errors associated with the connector model are considerably lower than those of the lattice-gas models. We attribute this accuracy to the inclusion of important high-order many-body interactions in the connector model, as well as to the fact that we were able to incorporate physically meaningful connectors into this model based on the insights gained from our detailed studies.

We note that, in addition to being more accurate than the lattice-gas model, the connector model is also more efficient computationally. For example, considering the six-atom cluster shown in Fig. 9(b) we would need 4N1, 3N2, 4N3, 2N4, 8T2, 4T3, 2T4, 2Q1, and 2Q2 (a total of 31 interactions) with the "best fit" ten-parameter lattice-gas model in Table II. In a Monte Carlo simulation, we would need to identify and sum these interactions. In contrast, only six connectors (4C6 and 2C7) are needed and, due to the simple form of the connector matrix, these are easy to identify in a MC simulation.

VI. CONCLUSIONS

In summary, we used the lattice-gas model and introduced the connector model to quantify interactions between Al adatoms on Al(110) and Al(100). In both of these systems, high-order many-body interactions are important in describing the energies of basic adsorbate configurations. We found the connector model to be more accurate for describing these systems. Because we were able to make some accurate simplifying assumptions in deriving the connector model, it will be more efficient than the lattice-gas model. Such simplifications may not be justified for more complex systems. However, the central idea of the connector model of combining groups of many-body interactions into important

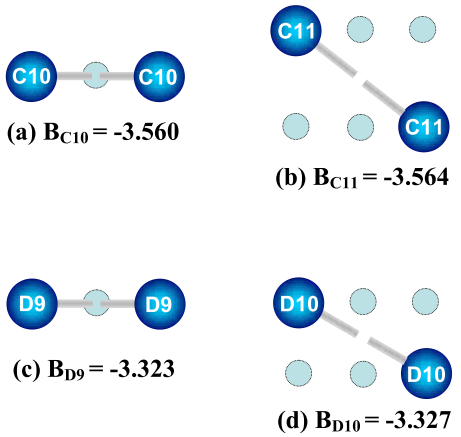

FIG. 11. (Color online) Connectors used to describe long-ranged pair interactions on [(a) and (b)] Al(110) and [(c) and (d)] Al(100) along with their binding energies. The small circles represent vacant sites.

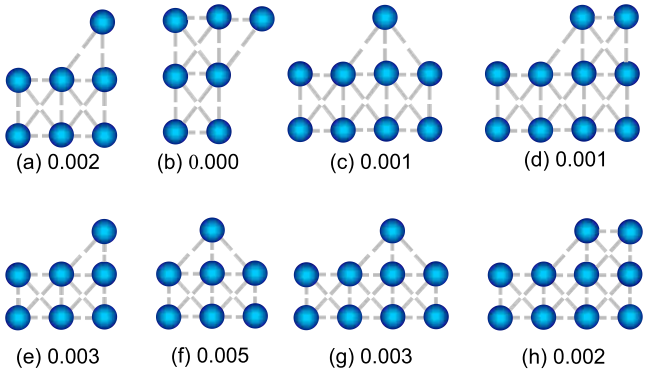

FIG. 12. (Color online) A few clusters which were used to test the connector matrix obtained for (a)–(d) Al(110) and (e)–(h) Al(100), along with the difference between the connector-model and DFT results (in eV/atom).

structural units (e.g., step edges) with a single interaction energy may be useful in future studies of thin-film and crystal growth, adsorption, phase transitions, and catalysis at surfaces.

ACKNOWLEDGMENT

This work was supported by the National Science Foundation under Grant No. DMR 0514336.

*fichthorn@psu.edu

[1] C. Stampfl, H. J. Kreuzer, S. H. Payne, H. Pfnür, and M. Scheffler, Phys. Rev. Lett. **83**, 2993 (1999).
[2] B. C. Han, A. Van der Ven, G. Ceder, and B.-J. Hwang, Phys. Rev. B **72**, 205409 (2005).
[3] Y. Zhang, V. Blum, and K. Reuter, Phys. Rev. B **75**, 235406 (2007).
[4] Y. Tiwary and K. A. Fichthorn, Phys. Rev. B **75**, 235451 (2007).
[5] R. Sathiyanarayanan, T. J. Stasevich, and T. L. Einstein, Surf. Sci. **602**, 1243 (2008).
[6] P. R. Schwoebel, S. M. Foiles, C. L. Bisson, and G. L. Kellogg, Phys. Rev. B **40**, 10639 (1989).
[7] J. Wintterlin, J. Trost, R. Schuster, A. Eichler, and J.-S. McEwen, Phys. Rev. Lett. **96**, 166102 (2006).
[8] A. P. J. Jansen and C. Popa, Phys. Rev. B **78**, 085404 (2008).
[9] L. Österlund, M. Ø. Pedersen, I. Stensgaard, E. Laegsgaard, and F. Besenbacher, Phys. Rev. Lett. **83**, 4812 (1999).
[10] F. Buatier de Mongeot, W. Zhu, A. Molle, R. Buzio, C. Boragno, U. Valbusa, E. G. Wang, and Z. Y. Zhang, Phys. Rev. Lett. **91**, 016102 (2003).
[11] A. Zunger, in *Statics and Dynamics of Alloy Phase Transformations*, NATO Advanced Studies Institute, Series B: Physics, edited by P. E. A. Turchy and A. Gonis (Plenum, New York, 1994).
[12] A. van de Walle and G. Ceder, J. Phase Equilib. **23**, 348 (2002).
[13] G. L. W. Hart, V. Blum, M. J. Walorski, and A. Zunger, Nature Mater. **4**, 391 (2005).
[14] N. A. Zarkevich and D. D. Johnson, Phys. Rev. Lett. **92**, 255702 (2004).
[15] R. Drautz and A. Díaz-Ortiz, Phys. Rev. B **73**, 224207 (2006).
[16] V. Blum and A. Zunger, Phys. Rev. B **69**, 020103(R) (2004).
[17] G. Kresse and J. Hafner, Phys. Rev. B **47**, 558 (1993).
[18] G. Kresse and J. Furthmüller, Comput. Mater. Sci. **6**, 15 (1996).
[19] G. Kresse and J. Furthmüller, Phys. Rev. B **54**, 11169 (1996).
[20] D. Vanderbilt, Phys. Rev. B **41**, 7892 (1990).
[21] G. Kresse and J. Hafner, J. Phys.: Condens. Matter **6**, 8245 (1994).
[22] J. P. Perdew and Y. Wang, Phys. Rev. B **45**, 13244 (1992).
[23] N. D. Mermin, Phys. Rev. **137**, A1441 (1965).
[24] H. J. Monkhorst and J. D. Pack, Phys. Rev. B **13**, 5188 (1976).
[25] *AIP Handbook*, 3rd ed., edited by D. E. Gray (McGraw-Hill, New York, 1972).
[26] R. Stumpf and M. Scheffler, Phys. Rev. B **53**, 4958 (1996).
[27] J. H. Petersen, A. Mikkelsen, M. M. Nielsen, and D. L. Adams, Phys. Rev. B **60**, 5963 (1999).
[28] S. J. Sferco, P. Blaha, and K. Schwarz, Phys. Rev. B **76**, 075428 (2007).
[29] V. Chis, B. Hellsing, G. Benedek, M. Bernasconi, and J. P. Toennies, J. Phys.: Condens. Matter **19**, 305011 (2007).
[30] J. L. F. Da Silva, Phys. Rev. B **71**, 195416 (2005).
[31] V. Chis and B. Hellsing, Phys. Rev. Lett. **93**, 226103 (2004).
[32] W. Berndt, D. Weick, C. Stampfl, A. M. Bradshaw, and M. Scheffler, Surf. Sci. **330**, 182 (1995).
[33] K. A. Fichthorn and M. Scheffler, Phys. Rev. Lett. **84**, 5371 (2000).
[34] W. Luo and K. A. Fichthorn, Phys. Rev. B **72**, 115433 (2005).
[35] T. J. Stasevich, T. L. Einstein, and S. Stolbov, Phys. Rev. B **73**, 115426 (2006).
[36] J. Koutecky, Trans. Faraday Soc. **54**, 1038 (1958).
[37] T. B. Grimley, J. Am. Chem. Soc. **90**, 3016 (1968).
[38] T. B. Grimley, Proc. Phys. Soc. London **90**, 751 (1967).
[39] T. B. Grimley, Proc. Phys. Soc. London **92**, 776 (1967).
[40] T. L. Einstein and J. R. Schrieffer, Phys. Rev. B **7**, 3629 (1973).
[41] K. H. Lau and W. Kohn, Surf. Sci. **65**, 607 (1977).
[42] K. H. Lau and W. Kohn, Surf. Sci. **75**, 69 (1978).
[43] T. L. Einstein, in *Chemistry and Physics of Solid Surfaces II*, edited by R. Vaneslow (CRC, Boca Raton, FL, 1979), p. 261.
[44] T. L. Einstein, Surf. Sci. **84**, L497 (1979).
[45] T. L. Einstein, in *Handbook of Surface Science*, edited by W. N. Unertl (Elsevier, Amsterdam, 1996), Vol. 1, p. 577.
[46] T. L. Einstein, Surf. Sci. **75**, 161 (1978).
[47] P. Hyldgaard and M. Persson, J. Phys.: Condens. Matter **12**, L13 (2000).
[48] P. Hyldgaard and T. L. Einstein, Europhys. Lett. **59**, 265 (2002).
[49] P. Hyldgaard and T. L. Einstein, Surf. Sci. **532-535**, 600 (2003).
[50] M. L. Merrick, W. Luo, and K. A. Fichthorn, Prog. Surf. Sci. **72**, 117 (2003).
[51] A. Bogicevic, S. Ovesson, P. Hyldgaard, B. I. Lundqvist, H. Brune, and D. R. Jennison, Phys. Rev. Lett. **85**, 1910 (2000).
[52] L. Vitos, H. L. Skriver, and J. Kollár, Surf. Sci. **425**, 212 (1999).
[53] P. Hecquet, B. Salanon, and B. Legrand, Surf. Sci. **459**, 23 (2000).
[54] F. Raouafi, C. Barreteau, M. C. Desjonquères, and D. Spanjaard, Surf. Sci. **505**, 183 (2002).
[55] J. L. F. DaSilva, C. Barreteau, K. Schroeder, and S. Blügel, Phys. Rev. B **73**, 125402 (2006).
[56] P. Stoltze, J. Phys.: Condens. Matter **6**, 9495 (1994).
[57] U. Hansen, P. Vogl, and V. Fiorentini, Phys. Rev. B **60**, 5055 (1999).
[58] M. Giesen, C. Steimer, and H. Ibach, Surf. Sci. **471**, 80 (2001).
[59] W. R. Tyson and W. A. Miller, Surf. Sci. **62**, 267 (1977).
[60] K. M. Ho and K. P. Bohnen, Phys. Rev. B **32**, 3446 (1985).
[61] G. Wulff, Z. Kristallogr. Mineral. **34**, 449 (1901).
[62] Z. Sun, Q. Liu, Y. Li, and J. Zhuang, Phys. Rev. B **72**, 115405 (2005).
[63] N. Memmel, E. Lægsgaard, I. Stensgaard, and F. Besenbacher, Phys. Rev. B **72**, 085411 (2005).
[64] K. Morgenstern, E. Lægsgaard, I. Stensgaard, and F. Besenbacher, Phys. Rev. Lett. **83**, 1613 (1999).
[65] D. R. Tice and D. W. Bassett, Thin Solid Films **20**, S37 (1974).
[66] D. W. Bassett, Thin Solid Films **48**, 237 (1978).